Am J Cancer Res 2016;6(2):509-521
www.ajcr.us /ISSN:2156-6976/ajcr0020405

*Original Article*

# Over expression of hyaluronan promotes progression of HCC via CD44-mediated pyruvate kinase M2 nuclear translocation

Jing-Huan Li[1,2*], Ying-Cong Wang[1,2*], Cheng-Dong Qin[1,2], Rong-Rong Yao[1,2], Rui Zhang[1,2], Yan Wang[1,2], Xiao-Ying Xie[1,2], Lan Zhang[1,2], Yan-Hong Wang[1,2], Zheng-Gang Ren[1,2]

*[1]Key Laboratory of Carcinogenesis and Cancer Invasion, Ministry of Education; [2]Liver Cancer Institute, Zhongshan Hospital, Fudan University, Shanghai 200032, China. [*]Equal contributors.*

Received December 7, 2015; Accepted December 18, 2015; Epub January 15, 2016; Published February 1, 2016

**Abstract:** Hyaluronan is expressed in hepatocellular carcinoma (HCC) as HCC generally arises from a cirrhotic liver in which excessive production and accumulation of HA leads to developing cirrhosis. Though it has been suggested HA is involved in progression of HCC, the mechanisms underlying the connection between HA and HCC progression are unclear. Since increased aerobic glycolysis is a metabolic trait of malignant cells and HA-CD44 can modulate glucose metabolism, we aim to investigate the roles of PKM2, a key enzyme in glucose metabolism, in the HA-CD44 axis facilitated the progress of HCC. We shown PKM2 was required for HA-promoted HCC progression, which was not modulated by PKM2 kinase activity but by nuclear translocation of PKM2. PKM2 translocation was Erk (Thr202/Tyr204) phosphorylation dependent, which functioned at the downstream of HA-CD44 binding. Furthermore, elevated HA expression significantly correlated with PKM2 nuclear location and was an independent factors predicting poor HCC prognosis. In conclusions PKM2 nuclear translocation is required for mediating the described HA biological effects on HCC progression and our results imply that inhibition of HA may have therapeutic value in treating HCC.

**Keywords:** Hepatocellular carcinoma, hyaluronan, CD44, pyruvate kinase M2

## Introduction

Hepatocellular carcinoma (HCC) is one of the most common cancers, especially where chronic hepatitis B infection is endemic. It ranks as the third most common cancer-related mortality worldwide and its prognosis is poor (a 5-year survival rate can be as low as 5%) [1]. Though a number of factors, including uncontrollable cancer cell growth and proliferation, cell energy metabolism, migration and metastasis, and angiogenesis are known to contribute to the virulence of cancer cells, effective block of HCC progression remains unknown.

Recent cancer biology study suggests that the extracellular matrix (ECM) is pleiotropic and has many more functions than just a structural scaffold since it can influence cellular destiny via various mechanisms [2]. Hyaluronan (HA), a member of the glycosaminoglycans, is produced by cell membrane binding proteins, such as the hyaluronan synthases (HASs) [3] and is expressed and released by cancer cells, especially by liver cancer cell [4].

Overexpression of the *has* gene and the accumulation of HA may relate to malignant transformation of cells [5]. Suppression of HA expression decreases tumor cell growth [6] and invasive capability [7], while increasing sensitivity to chemotherapy [8]. And HA levels are increased in patients with cirrhosis, which represents a pre-cancerous stage in the pathological process toward the HCC [9]. Thus, a clear understanding of the relationship between HA accumulation and HCC aggressiveness is of great need.

HA-induced effects are predominantly mediated through interactions with certain hyaladherins. CD44, is a common HA receptor, which is upregulated on the surface of some cancer cells and has been identified as a marker of

cancer stem cells [10]. HA-CD44 binding can trigger several signaling pathways such as PI3K/AKT, MEK [11], and Ras and RhoA signal pathways [12], leading to cancer progression. However, the specific signaling pathways triggered by HA-CD44 interaction in HCC cells have not yet been fully elucidated.

Increased aerobic glycolysis has been recognized as a metabolic trait of malignant cells and constitutes the metabolic basis of cancer progression. Previous studies have shown that HA and CD44 can modulate glucose metabolism and lactate efflux [13]. Pyruvate kinase M2 (PKM2), a key enzyme in glucose metabolism, is widely over-expressed in a variety of malignant tumors and is associated with tumorigenicity, tumor proliferation and progression. Different to pyruvate kinase M1, PKM2 has a lower affinity to phosphoenolpyruvate and is modulated by a growth factor through tyrosine phosphorylation, resulting in reduced activity because of repression of binding of fructose-1, 6-bisphosphate with PKM2 [14]. CD44 as a co-activator of many growth factor receptors promotes tumor proliferation and metastasis in various cancers. The role of CD44 in PKM2 modulation and its subsequent biological action in tumor progression has not been clarified.

In this study, we aimed to investigate the effects of HA on facilitating the aggressive phenotype of HCC cell lines and the underlying mechanism in both *in vitro* and *in vivo* studies as well as an analysis of clinical HCC samples. We initially identified PKM2 as a downstream factor of HA-CD44 signaling, which induced extracellularly regulated protein kinases (ERK)-dependent PKM2 nuclear translocation, that was involved in HA-promoted HCC proliferation, metastasis potential and aerobic glycolysis switch.

## Materials and methods

### *Cell lines and culture*

The human HCC cell line MHCC97H was established in the Liver Cancer Institute, Fudan University [15]. HepG2 was obtained from the Chinese Academy of Sciences Shanghai Branch, China. The cell lines were cultured in DMEM with high glucose (Life technologies) supplemented with 10% fetal bovine serum (Life technologies), 100 IU/ml penicillin G and 100 mg/ml streptomycin sulfate (Sigma-Aldrich) at 37°C in a humidified atmosphere containing 5% $CO_2$.

### *Lentivirus and tranfection*

Four lentiviruses were established by Hanyin Biotechnology, Shanghai, China: an empty vector control (Control), stable knockdown of PKM2 (shPKM2), overexpressed PKM2 (PKM2 OE), and a PKM2 Ser37A mutation (PKM2 Ser37A) [16]. All transfections were performed according to the manufacturer's protocols. Detailed lentiviruses establishment protocols were described in the Supplementary Material.

### *Western blot analysis, quantitative real-time PCR, and immunofluorescence*

Detailed protocols were described in the Supplementary Material.

The RT-PCR primers were synthesized with following sequences: PKM2, 5'-GCTGCCATCTACCACTTGC-3' (forward) and 5'-CCAGACTTGGTGAGGACGATT-3' (reverse); GAPDH, 5'-GCACCGTCAAGGCTGAGAAC-3' (forward) and 5'-TGGTGAAGAACGCCAGTGGA-3' (reverse).

### *Cell proliferation, colony formation, cell migration, and invasion*

Detailed protocols were described in the Supplementary Material.

### *Measurements of aerobic glycolysis and pyruvate kinase activity*

Detailed protocols were described in the Supplementary Material. A lucose assay kit and Lactate assay kit (MAK013 and MAK064, Sigma-Aldrich) were used to determine the levels of glucose and lactate respectively. Glucose consumption was the difference in glucose concentration when compared with DMEM. The activity of PK was measured with a Pyruvate kinase assay (MAK072, Sigma-Aldrich) according to the manufacturer's instruction.

### *Evaluation of tumor growth in vivo*

The animal experiments were carried out in accordance with the guideline of the Shanghai Medical Experimental Animal Care Commission and all animals received human care. Detailed protocols were described in the Supplementary Material. Briefly, cells ($5\times10^6$ per 200 μl Matrigel (1:8 diluted, 354263, BD Biosciences,

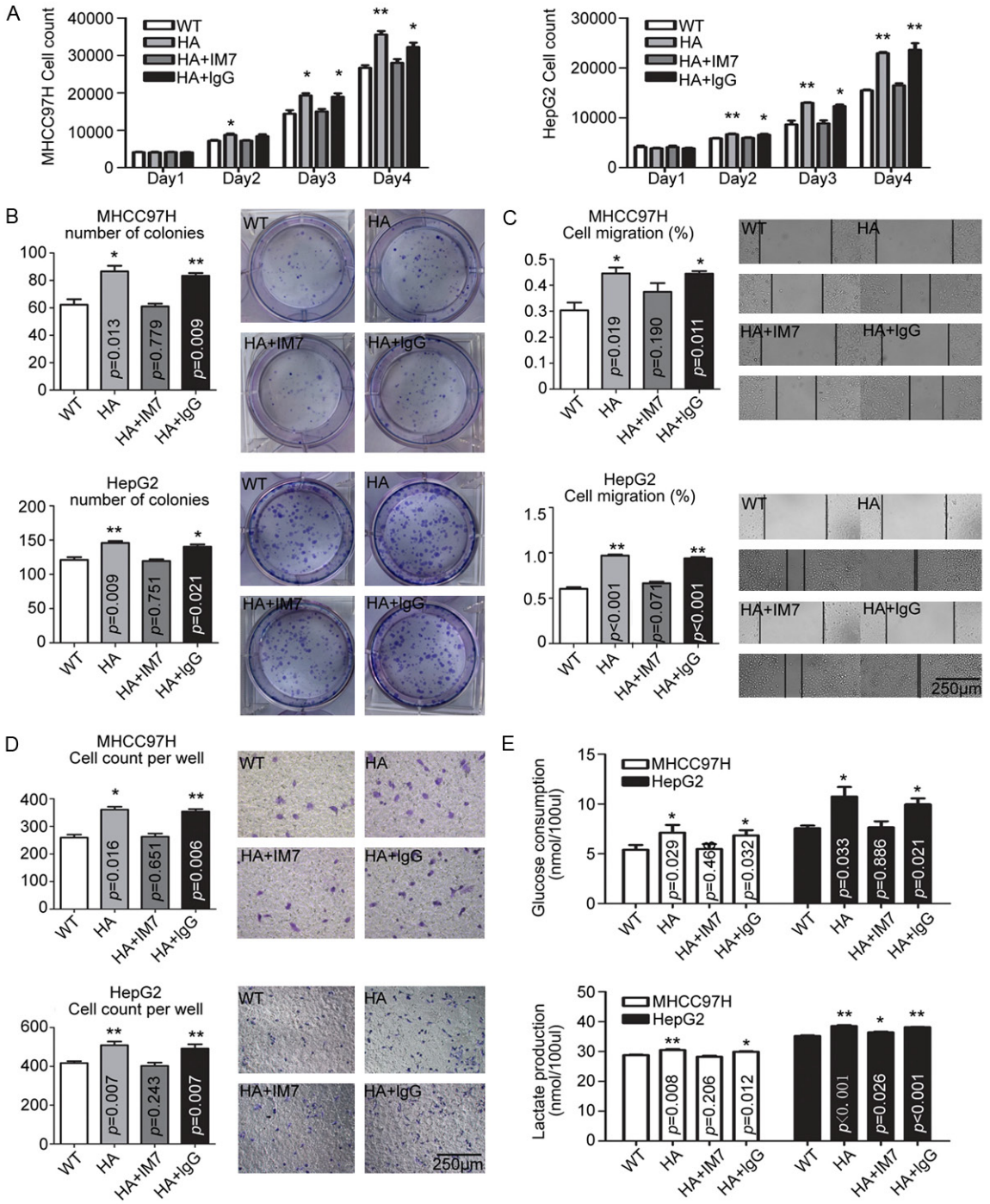


**Figure 1.** Effect of HA stimulation on HCC cell lines. In MHCC97H and HepG2 cells, HA promoted cells proliferation (A), colony formation capacity (B), migration potential (C, D), and aerobic glycolysis switch (E), which effects were abolished by CD44 blocking antibody IM7, but not by non-specific IgG. The data were plotted with the mean+SD of three different experiments. * $p<0.05$. ** $p<0.01$.

CA) with 100 μg/ml HA (GLR003, R&D systems)) were subcutaneously injected. The mice were euthanized after 4 weeks. The tumor volume was calculated by (large diameter) × (small diameter)$^2$/2.

*Patients and immunohistochemistry of tissue microarrays (TMAs)*

This study was approved by the Institutional Review Board of Zhongshan Hospital and writ-

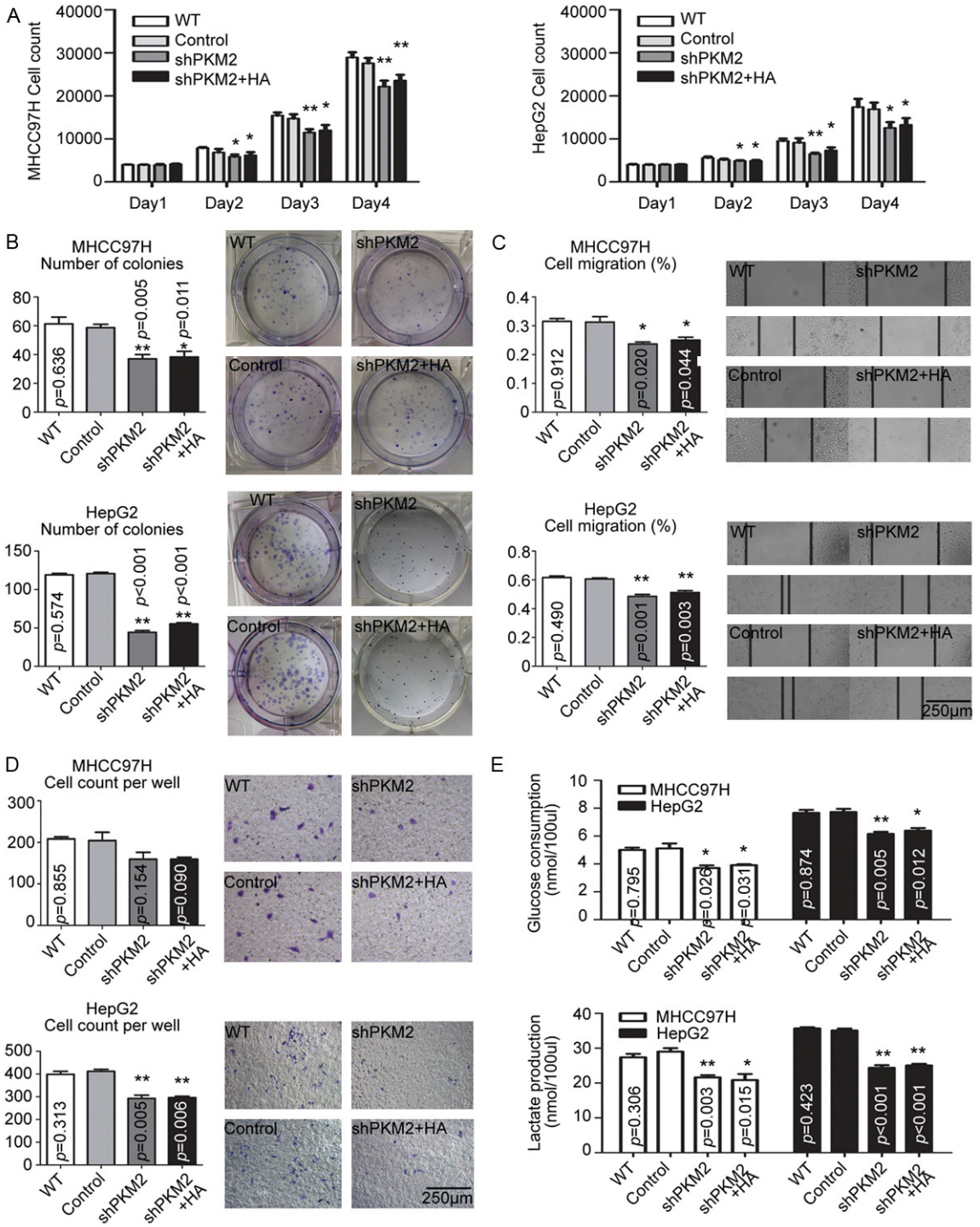


**Figure 2.** PKM2 was involved in HA-promoted HCC cell proliferation, metastasis potential and aerobic glycolysis switch. In MHCC97H and HepG2 cells, silencing PKM2 reduced cell proliferation (A), colony formation (B), migration potential (C, D), and aerobic glycolysis switch (E), as well as the response to HA stimulus. The data were plotted with the mean+SD of three different experiments. * $p<0.05$. ** $p<0.01$.

ten informed consent was obtained from all patients. A total of 105 HCC tissues from patients who had curative resection from Jan, 2008 to Dec, 2008 at Liver Cancer Institute,

Zhongshan Hospital, Fudan University, Shanghai, China, were analyzed using TMAs. Patient follow-up was completed in March, 2014. The median follow-up period was 58 months (±19.9, range 12-76 months).

The detail of generating these TMAs and immunohistochemistry protocol were described in Supplementary Material.

The photographs of 4 representative fields were captured by Leica QWin Plus v3 software, and the integrated optical density (IOD) values of those photographs were measured by Image-Pro Plus v6.0 software. X-tile software program was used to identify the significant cut-off point of certain protein expression levels in terms of overall survival. If more than 50% cells had PKM2 located in the nucleus, the samples were categorized as nuclear PKM2 positive. A uniform setting was applied for all the slides when reading each antibody staining.

*Statistical analysis*

The data were expressed as mean ± standard deviation. The association between variables was analyzed using Student's t test, Mann-Whitney U test or Fisher's exact test when appropriate. Variables associated with Prognosis were identified using univariable Cox proportional hazards regression models. Significant factors in univariable analysis were further subjected to a multivariable Cox regression analysis in a backward manner. Overall survival (OS) was measured from time of resection until death from any cause or until the last date of follow up. Data were censored for patients who remained alive at the end of the study. Kaplan-Meier plots (log-rank test) were used to describe OS. Two-sided $p<0.05$ was considered a significant result. Statistical analyses were performed with SPSS 19.0 for windows.

## Results

*HA promoted the cell proliferation, metastasis potential and aerobic glycolysis switch in MHCC97H and HepG2 cells*

First, we evaluated the effects of HA on the proliferation in MHCC97H and HepG2 which have different metastasis potential. Different concentrations of HA (50, 100, 150, 200 μg/ml) were included in the HepG2 cell proliferation assay. Compared with the control group, all four HA concentrations promoted the proliferation of HepG2 cells (Day 4: $p<0.001$ all four group vs Control). HA at 100 μg/ml led to significantly higher proliferation of HepG2 cells compared with 50 μg/ml HA (Day 4: $p<0.001$), while HA at 150 or 200 μg/ml shown similar effects on cell proliferation to HA at 100 μg/ml (Day 3: $p=0.051$, $p=0.862$; Day 4: $p=0.011$, $p=0.206$) (Supplementary Figure 1A). Second, we also noted that HA at 100 μg/ml significantly promoted the proliferation of MHCC97H cells (Day 4: $p=0.001$) (**Figure 1A**). Thus, the 100 μg/ml concentration was chosen for use in experiments of the two HCC cell lines.

The impact of HA on colony formation capacity of HCC cells was next examined. The number of colonies of MHCC97H and HepG2 cells after HA treatment was significantly higher compared to the control group (**Figure 1B**). Furthermore, the ability of migration and invasion of cells was higher by including HA treatment (**Figure 1C** and **1D**).

It has been suggested that aerobic glycolysis is associated with increased anabolic metabolism in rapid proliferative cancer cells [13], including HCC [17], and CD44, the most common receptor for HA, is involved in modulating glucose metabolism [13]. Therefore, we further examined cellular glycolysis after HA stimulation. By measuring glucose consumption and lactate production which partially reflects the status of glycolysis, we found HA significantly increased the glucose consumption and lactate production in HCC cells (**Figure 1E**).

To verify whether the effects of HA were mediated by CD44, we analyzed CD44 expression by flow cytometry. Results revealed a high percentage of cells were positive for CD44 in both MHCC97H and HepG2 cells (Supplementary Figure 1B). Using a CD44 blocking antibody IM7 [18], we found that the promotion of proliferation, metastasis potential, and aerobic glycolysis switch of HA were abolished by IM7, but not by non-specific IgG, suggesting the effects of HA on HCC cells were mediated by interacting with CD44 (**Figure 1**).

*PKM2 plays an essential role in HA-CD44 promoted progression in HCC cells*

Given that PKM2 is a key enzyme in cancer aerobic glycolysis and that the role of CD44 in

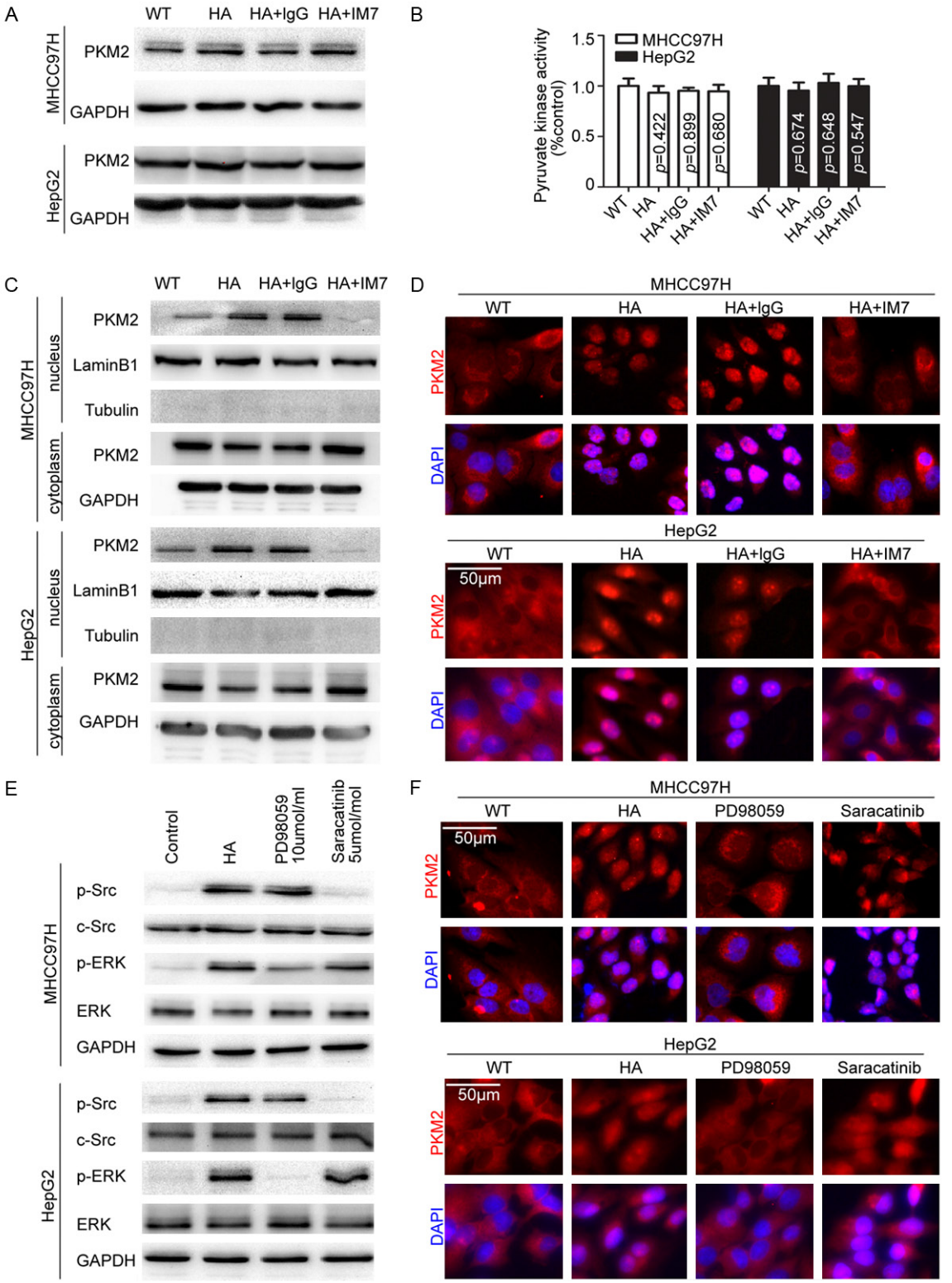


**Figure 3.** HA stimulated PKM2 nuclear translocation through ERK pathway activation. A. Total PKM2 was detected under different stimulations, suggesting HA stimulus had no effect on PKM2 expression levels. B. HA stimulus had no effect on total PK activity of HCC cells. C. Nuclear protein was extracted. HA-CD44 binding led to PKM2 nuclear translocation. Lamin B was used as loading controls. D. Immunofluorescence shown HA-CD44 binding led to PKM2 nuclear translocation. E. HA stimulus activated Src (phosphor-Src Tyr416) and ERK (phosphor-p44/42 MAPK Thr202/Tyr204). The efficiency of Src and ERK inhibitor were detected. F. Blocking ERK activation could inhibit HA-induced PKM2 nuclear translocation.

modulation of glycolysis [13], we examined whether PKM2 was required for HA-CD44 promoted HCCs progression *in vitro*. MHCC97H and HepG2 cells were transfected with lentivirus vectors, resulting in the stable knockdown of PKM2 (Supplementary Figure 1C).

As shown in **Figure 2**, the knockdown of PKM2 significantly reduced the response to HA stimulus as seen with reduced cell proliferation, colony formation, migration, invasion, and increased glucose consumption in both MHCC97H and HepG2 cells, but there was no reduced response in the control group, compared with the wild type cells.

*HA-CD44 binding leads to ERK-dependent PKM2 nuclear translocation*

The aforementioned results suggested PKM2 mediated HA-induced HCC progression. We further examined the expression of PKM2 and the pyruvate kinase activity in HCC cells. No clear changes were observed in the overall PKM2 expression and pyruvate kinase activity in those cells (**Figure 3A** and **3B**). However, Western blot and Immunofluorescence PKM2 was translocated to the nucleus following 6 hours of HA stimulation in both MHCC97H and HepG2 cells (**Figure 3C** and **3D**). Thus, it would appear that HA-CD44 binding led to PKM2 nuclear translocation but did not involve alterations in PKM2 activity or expression.

To further identify the signal involved in PKM2 nuclear translocation, we explored the downstream signal of HA-CD44. Consist with previous studies [19, 20], we examined and found c-Src and ERK were significantly activated at 30 minutes following HA stimulation (Supplementary Figure 1D and 1E). Then, treated the cells with c-Src kinase inhibitor (AZD0530, a gift from AstraZeneca) or MEK kinase inhibitor (PD98059, Selleck), we found only the inhibition of ERK activation blocked the nuclear translocation of PKM2, but no significant effects were observed after inhibition of c-Src, indicating the activation of MEK/ERK following HA stimulation mediated PKM2 nuclear translocation (**Figure 3E**, **3F**. and Supplementary Figure 1F).

*PKM2 nuclear translocation was critical for the HA-stimulated HCC progression in vitro and tumor growth in vivo*

Considering the aforementioned data, however, whether PKM2 enzymatic activity or just PKM2 nuclear translocation mediated the HA-CD44 promoted HCC progression was not clarified. To clarify the issue, we constructed a lentivirus vector carrying flag-tagged PKM2 with Ser37A mutant and then transfected the lentivirus into MHCC97H and HepG2 since It has been reported that phosphorylated PKM2 Ser 37 is required for PKM2 translocation to the nucleus [16]. As shown in **Figure 4A**, **4B**. and Supplementary Figure 1G, a PKM2 Ser37A mutant that was expressed in HCC cells was resistant to HA-induced nuclear translocation.

Similar to the shPKM2 cells, the expression of the PKM2 mutant blocked the aggressive behaviors of HCC cells as well as leading to a diminished response to HA stimulation when comparing control group (**Figure 4C-G**), which suggested that PKM2 nuclear translocation was required for HCC progression and aerobic glycolysis upon HA stimulation.

Furthermore, the role of PKM2 in promoting HA-stimulated HCC cell growth was corroborated *in vivo*. The MHCC97H cells with shPKM2 or PKM2 mutant were implanted subcutaneously in nude mice together with Matrigel and HA. Tumor growth in the mice with shPKM2 or PKM2 mutant were significantly retarded compared with controls (1.33±0.11 vs 2.07±0.16 $cm^3$, $p$=0.004 and 1.53±0.15 vs 2.07±0.16 $cm^3$, $p$=0.038 respectively, **Figure 4H**). Conversely, the mice implanted with MHCC97H cells with PKM2 over-expression (PKM2 OE) formed larger tumors subcutaneously (2.30± 0.20 vs 2.07±0.16 $cm^3$, $p$=0.424, **Figure 4H**).

*HA expression correlated with PKM2 nuclear localization and HA overexpression and PKM2 nuclear localization were closely related to poor prognosis of HCC*

Considering the biological effects of HA on HCC cells, we analyzed clinical data and explored the HA relevance to HCC progression. The expression of HA was immunohistochemically evaluated in 105 primary HCC cancer samples that were paired with normal liver tissues. As defined in materials and methods, high HA expression was detected in 49 (46.7%) of 105 tumor tissues (typical low and high HA expression are shown in **Figure 5A**), and tumor tissues exhibited significantly higher expression of HA compared with paired normal liver tissues ($p$<0.001, **Figure 5B**). HCC patients with elevated HA expression was significantly associated with poor overall survival ($p$<0.001, **Figure 5C**).

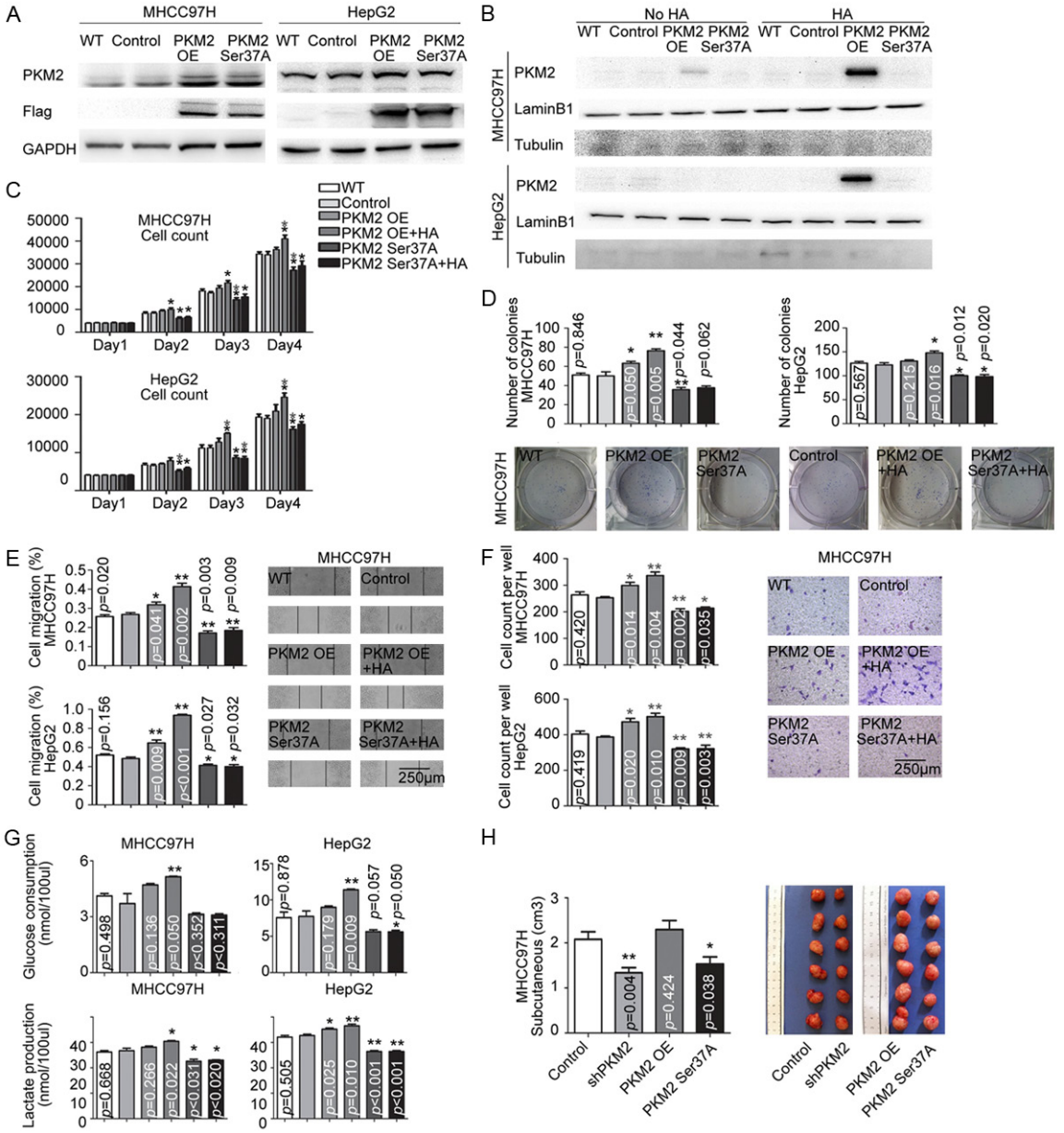


**Figure 4.** PKM2 nuclear translocation was crucial for HA-stimulated HCC progression. (A) The efficiency of flag-tagged lentivirus transfection was detected. PKM2 OE is short for PKM2 overexpression, PKM2 Ser37A is short for PKM2 Ser37 mutation. (B) Nuclear protein was extracted. PKM2 Ser37 mutation inhibited the nuclear translocation of PKM2. In MHCC97H and HepG2 cells, Mutated PKM2Ser37 reduced cell proliferation (C), colony formation (D), migration potential (E, F), and increased glucose consumption (G), as well as the response to HA stimulus. (H) Cells with different expression levels of PKM2 were subcutaneously implanted with HA. Tumor volumes were measured (n=6).

Further, we evaluated the correlation between the expression of HA, clinical features and biological markers of patients. As summarized in **Table 1**, high HA expression significantly correlated with large tumor size and poor tumor differentiation ($p$=0.019 and $p$=0.001, respectively).

Considering that HA-induced PKM2 nuclear translocation is important in the HA-CD44 signaling pathway, we investigated the pattern of PKM2 expression. As defined in materials and methods, it shown 40 of 105 samples (38.1%) had high PKM2 expression. And 47 (44.8%) tumor tissues had PKM2 located in the nucle-

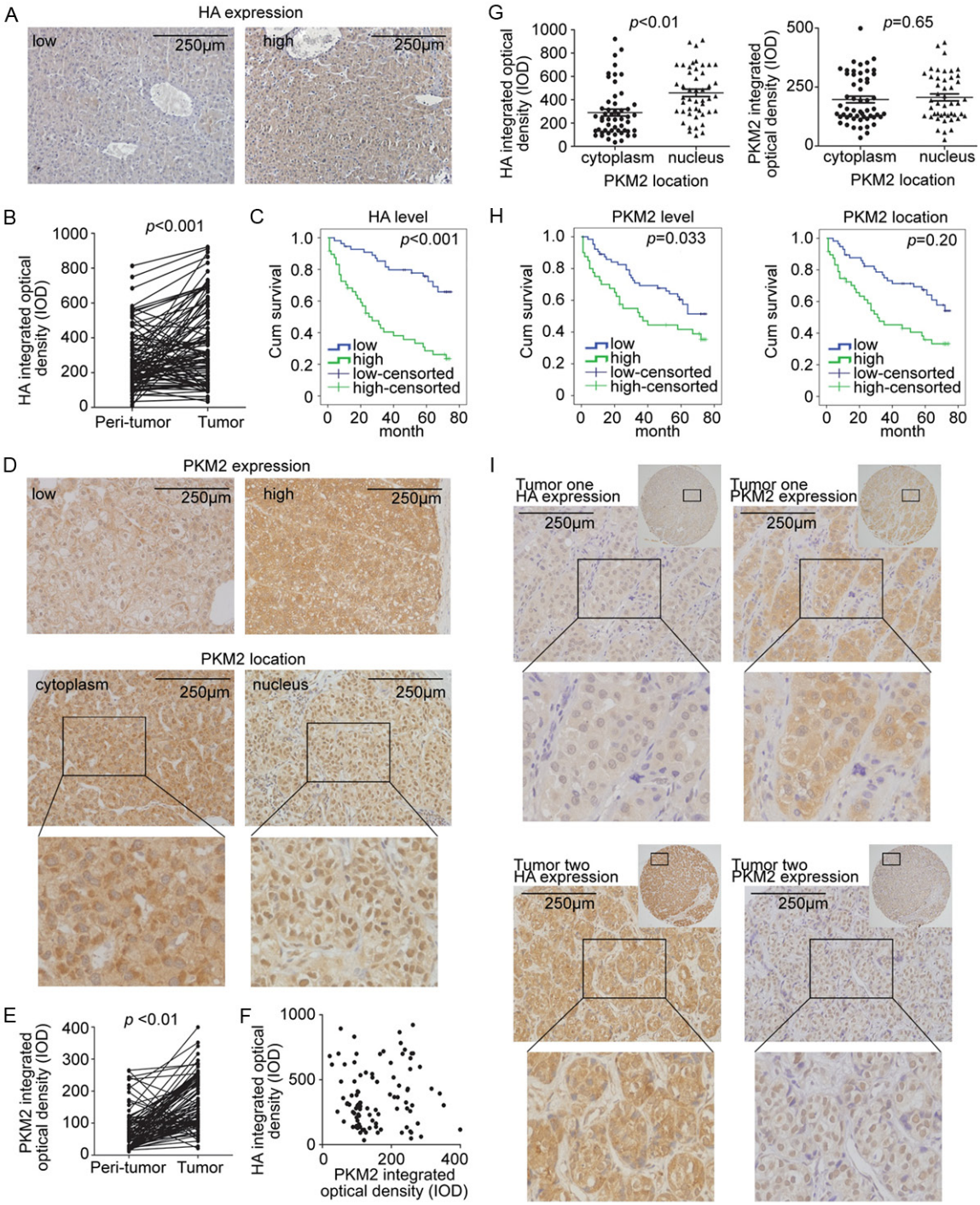


**Figure 5.** Elevated HA related to PKM2 nuclear localization and poor prognosis of HCC. A. Typical weak/strong staining of HA. B. Tumor tissues exhibited higher HA expression. C. Survival curves for OS according to HA expression level. D. Typical staining of PKM2: weak/strong (upper panel); cytoplasm/nucleus location (bottom panel). E. Tumor tissues exhibited higher PKM2 expression. F. No clear correlation between HA and PKM2 expression. G. PKM2 nuclear localization correlated with the HA, but not PKM2 staining densities. H. Survival curves for OS according to PKM2 expression level or PKM2 location. I. Two typical tissues that reflected the correlation between HA and PKM2 expression.

us, while the dominant PKM2 nuclear translocation was not detected in a single normal liver tissue (typical expression are shown in **Figure 5D**). Compared with paired normal liver tissues,

**Table 1.** Association of HA expression and PKM2 subcellular localization with clinicopathological characteristics in HCC (n=105)

| Charactieristic | n | HA high | *p* | PKM2 high | *p* | Nuclear PKM2 | *p* |
|---|---|---|---|---|---|---|---|
| Total | 105 | 49 (46.7%) | | 40 (38.1%) | | 47 (44.8%) | |
| Gender | | | | | | | |
| Male | 87 (82.9%) | 37 (42.5%) | | 32 (36.8%) | | 37 (42.5%) | |
| Female | 18 (17.1%) | 2 (11.1%) | 0.671 | 8 (44.4%) | 0.548 | 10 (55.6%) | 0.549 |
| Age | | | | | | | |
| ≤60 | 70 (66.7%) | 34 (48.6%) | | 28 (40.0%) | | 31 (44.3%) | |
| >60 | 35 (33.3%) | 15 (42.9%) | 0.81 | 12 (34.3%) | 0.139 | 16 (45.7%) | 0.872 |
| HBsAg | | | | | | | |
| No | 22 (20.9%) | 7 (31.8%) | | 6 (27.3%) | | 11 (50.0%) | |
| Yes | 83 (79.1%) | 42 (50.6%) | 0.262 | 44 (53.0%) | 0.21 | 36 (43.4%) | 0.78 |
| Liver cirrhosis | | | | | | | |
| No | 24 (22.9%) | 10 (41.7%) | | 8 (33.3%) | | 8 (33.3%) | |
| Yes | 81 (77.1%) | 39 (48.1%) | 0.593 | 32 (39.5%) | 0.784 | 39 (48.1%) | 0.293 |
| Serum AFP (ng/ml) | | | | | | | |
| ≤20 | 53 (50.5%) | 24 (45.3%) | | 16 (30.2%) | | 19 (35.8%) | |
| >20 | 52 (49.5%) | 25 (48.1%) | 0.821 | 24 (46.2%) | 0.244 | 28 (53.8%) | 0.172 |
| Tumor size (cm) | | | | | | | |
| ≤5 | 51 (48.6%) | 18 (36.7%) | | 19 (37.3%) | | 20 (39.2%) | |
| >5 | 54 (51.4%) | 31 (63.3%) | 0.019* | 21 (38.9%) | 0.819 | 27 (50.0%) | 0.372 |
| Tumor number | | | | | | | |
| Single | 87 (82.9%) | 39 (44.8%) | | 32 (36.8%) | | 39 (44.8%) | |
| Multiple | 18 (17.1%) | 10 (55.6%) | 0.56 | 8 (44.4%) | 0.548 | 8 (44.4%) | 0.919 |
| Tumor encapsulation | | | | | | | |
| Yes | 63 (60.0%) | 27 (42.9%) | | 26 (37.7%) | | 34 (55.7%) | |
| No | 42 (40.0%) | 22 (52.4%) | 0.491 | 14 (38.9%) | 0.81 | 8 (38.1%) | 0.103 |
| Vascular invasion | | | | | | | |
| No | 69 (65.7%) | 30 (43.5%) | | 17 (27%) | | 24 (34.8%) | |
| Yes | 36 (34.3%) | 19 (52.8%) | 0.484 | 23 (54.8%) | 0.015* | 23 (63.9%) | 0.043* |
| Tumor differentiation | | | | | | | |
| I/II | 85 (81.0%) | 31 (36.5%) | | 31 (36.5%) | | 35 (41.2%) | |
| III/IV | 20 (19.0%) | 18 (90.0%) | 0.001* | 9 (45.0%) | 0.241 | 12 (60.0%) | 0.251 |
| TNM stage | | | | | | | |
| I | 49 (46.7%) | 22 (44.9%) | | 19 (38.8%) | | 20 (69.0%) | |
| II/III | 56 (53.3%) | 27 (48.2%) | 0.823 | 21 (37.5%) | 0.943 | 27 (48.2%) | 0.652 |

*$p<0.05$. Abbreviations: HBsAg, hepatitis B surface antigen; AFP, alpha-fetoprotein; TNM, tumor-node-metastasis.

the tumor tissues exhibited significantly higher expression of PKM2 ($p<0.001$, **Figure 5E**).

We then analyzed whether PKM2 nuclear location was associated with HA expression level. In line with our *in vitro* study aforementioned, there was no clear correlation between HA expression and total PKM2 expression levels (**Figure 5F**). Moreover, PKM2 nuclear location correlated with HA expression, but not total PKM2 expression level (**Figure 5G**). (Two typical tissues that reflected the correlation between HA and PKM2 expression was shown in **Figure 5I**).

We also analyzed potential HCC prognostic factors through univariate and multivariate analysis. Six factors were significantly associated with overall survival, including high HA expression, PKM2 expression, PKM2 nuclear location,

**Table 2.** Univariate and multivariate analyses of prognostic factors affecting OS (n=105)

| | | Multivariate | |
|---|---|---|---|
| Variables | Univariate *p* | HR (95.0% CI) | *p* |
| HA expression | 0.000* | 2.468 (1.041-5.851) | 0.040* |
| PKM2 expression | 0.033* | 1.826 (0.904-3.688) | 0.093 |
| PKM2 nuclear vs cytoplasm | 0.020* | 1.713 (0.803-3.658) | 0.164 |
| Age, >60 vs. ≤60 years | 0.514 | | |
| Gender, Male vs. Female | 0.002* | 1.964 (0.791-4.876) | 0.146 |
| HBsAg, Positive vs. negative | 0.467 | | |
| Liver cirrhosis, Yes vs. No | 0.353 | | |
| Serum AFP, >20 vs. ≤20 ng/mL | 0.460 | | |
| Tumor size, >5 vs. ≤5 cm | 0.001* | 2.488 (1.202-5.148) | 0.014* |
| Tumor number, Multiple vs. Single | 0.164 | | |
| Tumor encapsulation, No vs. Yes | 0.642 | | |
| Vascular invasion, Yes vs. No | 0.006* | 1.859 (0.941-3.671) | 0.074 |
| Tumor differentiation, III/IV vs. I/II | 0.394 | | |
| TNM stage, II/III vs. I | 0.055 | | |

*$p<0.05$. Abbreviations: HBsAg, hepatitis B surface antigen; AFP, alpha-fetoprotein; TNM, tumor-node-metastasis; HR, hazard ratio; CI, confidence interval.

male gender, tumor diameter larger than 5 cm, and vascular invasion (**Table 2**, **Figure 5C** and **5H**). Further multivariate analysis shown that high HA expression and tumor diameter larger than 5 cm were independent prognostic factors that significantly affected overall survival ($p$=0.040 and $p$=0.014, respectively).

## Discussion

This study revealed the mechanism of HA-promoted HCC progression through ERK-dependent PKM2 nuclear translocation.

We found the significantly stronger ability of cancer cell proliferation and migration potential was associated with higher HA expression levels. Some studies have explored the mechanisms of HA and its role in promoting tumor progression. Kharaishvili et al. revealed that excessive HA accumulation in ECM may dilute tissue compression, which surrounds cancer cells, owing to its electrostatic repulsion and ability to trap water [21]. It is likely that the loose and hydrated nature of HA facilitates cancer cell proliferation and expansion. Furthermore, HA also has anti-adhesive properties permitting tumor cells to be released from the primary tumor mass. However, given that HA could reflect the state of liver cirrhosis which is considered a pre-cancerous condition, the hydrated microenvironment caused by HA accumulation might be linked to increased tumor tissue stiffness [21], which has been shown to be associated with HCC development [22]. Other related mechanisms include HA's ability to increase extravascular stress mainly by elevating interstitial fluid pressures [23], while Chauhan et al. argued that HA is the major determinant of solid stress [24].

We also found excessive expression of HA abnormally up-regulated aerobic glycolysis in parallel with progression of cancer cells. When comparing normal adults cells, cancer cells are more likely to show altered metabolic patterns in which they assimilate more glucose and process it primarily into lactate through aerobic glycolysis [25]. Thus, cancer cells attained metabolic advantages for cell proliferation and division [25].

We further studied the mechanisms underlying HA-induced HCC progression. We shown for the first time that PKM2 nuclear translocation was required to progress HA-induced HCC progression. Furthermore, the MEK/ERK axis was strongly associated with effects of HA on PKM2 nuclear translocation in HCC cells. Our results corroborate recent findings focusing on other tumor cells, in which PKM2 could endow cancer cells with a malignant phenotype by translocating to the nucleus. Once in the nucleus, PKM2 phosphorylated specific nuclear proteins, such as β-catenin, HIF-1 and STAT3, and activated transcription of various genes [26].

It has been reported that HA-CD44 binding selectively led to an enhanced activity of the cell cycle regulatory genes such as CYCLIN D1 in a MAPK and Akt dependent manner [19, 27]. Also, HA binding to CD44 specifically stimulated the Wnt/β-catenin pathway in promoting proliferation and invasion of cells [28, 29]. However, the molecules that mediated the sig-

naling of HA-CD44 down-stream were not identified. Our study provided evidence that PKM2, a well-recognized co-activator of β-catenin, could partially mediate the effects of HA on β-catenin activity, consequently leading to HCC progression. To some extent, our findings supported the previous observations, in which HA was found to regulate the activation of HIF-1 and STAT3 [30, 31]. PKM2 may serves as a possible bridge between HA signaling and the activation of cancer related genes in transcription.

Recently, HA has emerged as a promising therapeutic target for cancer therapy. The HA synthesis inhibitor, 4-methylumbelliferone [6] and the enzymatic agent, PEGPH20 (pegylated human recombinant hyaloronidase) [32] were both found to decrease HA expression and led to strong inhibition of tumor development *in vivo*. However, in view of ubiquitous expression of HA in human various organs, improving the specificity of anti-tumor effects and the minimizing of side-effects are required. Our study shown that PKM2, another recently emerging cancer therapeutic target, was a crucial factor located downstream of HA, providing a potential co-target for cancer drug development.

In summary, we found the HCC cells treated with HA exhibited aggressive properties of proliferation, migration and energy metabolism *in vitro*. And PKM2 nuclear translocation was required to progress HA-induced HCC progression. Further, we analyzed the clinical data and shown that HA overexpression correlated with PKM2 nuclear localization and poor prognosis of HCC. These findings suggest that target HA is a promising treatment of HCC.

## Acknowledgements

This study was supported by National Clinical Key Special Subject of China and Nation Natural Science Foundation of China (81172275 and 81272565).

## Disclosure of conflict of interest

None.

**Address correspondence to:** Zheng-Gang Ren and Yan-Hong Wang, Zhongshan Hospital, Fudan University, Shanghai 200032, China. Tel: 021-64041990; E-mail: ren.zhenggang@zs-hospital.sh.cn (ZGR); wang.yanhong@zs-hospital.sh.cn (YHW)

## References

[1] Torre LA, Bray F, Siegel RL, Ferlay J, Lortet-Tieulent J, Jemal A. Global cancer statistics, 2012. CA Cancer J Clin 2015; 65: 87-108.

[2] Oskarsson T. Extracellular matrix components in breast cancer progression and metastasis. Breast 2013; 22 Suppl 2: S66-S72.

[3] Vigetti D, Viola M, Karousou E, De Luca G, Passi A. Metabolic control of hyaluronan synthases. Matrix Biol 2014; 35: 8-13.

[4] Vigetti D, Karousou E, Viola M, Deleonibus S, De Luca G, Passi A. Hyaluronan: biosynthesis and signaling. Biochim Biophys Acta 2014; 1840: 2452-2459.

[5] Okuda H, Kobayashi A, Xia B, Watabe M, Pai SK, Hirota S, Xing F, Liu W, Pandey RR, Fukuda K, Modur V, Ghosh A, Wilber A, Watabe K. Hyaluronan synthase HAS2 promotes tumor progression in bone by stimulating the interaction of breast cancer stem-like cells with macrophages and stromal cells. Cancer Res 2012; 72: 537-547.

[6] Lokeshwar VB, Lopez LE, Munoz D, Chi A, Shirodkar SP, Lokeshwar SD, Escudero DO, Dhir N, Altman N. Antitumor activity of hyaluronic acid synthesis inhibitor 4-methylumbelliferone in prostate cancer cells. Cancer Res 2010; 70: 2613-2623.

[7] Bernert B, Porsch H, Heldin P. Hyaluronan synthase 2 (HAS2) promotes breast cancer cell invasion by suppression of tissue metalloproteinase inhibitor 1 (TIMP-1). J Biol Chem 2011; 286: 42349-42359.

[8] Wang SJ, Earle C, Wong G, Bourguignon LY. Role of hyaluronan synthase 2 to promote CD44-dependent oral cavity squamous cell carcinoma progression. Head Neck 2013; 35: 511-520.

[9] Piccioni F, Malvicini M, Garcia MG, Rodriguez A, Atorrasagasti C, Kippes N, Buena IT, Rizzo MM, Bayo J, Aquino J, Viola M, Passi A, Alaniz L, Mazzolini G. Antitumor effects of hyaluronic acid inhibitor 4-methylumbelliferone in an orthotopic hepatocellular carcinoma model in mice. Glycobiology 2012; 22: 400-410.

[10] Karbownik MS, Nowak JZ. Hyaluronan: towards novel anti-cancer therapeutics. Pharmacol Rep 2013; 65: 1056-1074.

[11] Herishanu Y, Gibellini F, Njuguna N, Hazan-Halevy I, Farooqui M, Bern S, Keyvanfar K, Lee E, Wilson W, Wiestner A. Activation of CD44, a receptor for extracellular matrix components, protects chronic lymphocytic leukemia cells from spontaneous and drug induced apoptosis through MCL-1. Leuk Lymphoma 2011; 52: 1758-1769.

[12] Wang SJ, Bourguignon LY. Role of hyaluronan-mediated CD44 signaling in head and neck

squamous cell carcinoma progression and chemoresistance. Am J Pathol 2011; 178: 956-963.
[13] Tamada M, Nagano O, Tateyama S, Ohmura M, Yae T, Ishimoto T, Sugihara E, Onishi N, Yamamoto T, Yanagawa H, Suematsu M, Saya H. Modulation of glucose metabolism by CD44 contributes to antioxidant status and drug resistance in cancer cells. Cancer Res 2012; 72: 1438-1448.
[14] Gao XL, Wang HZ, Yang JJ, Chen J, Jie J, Li LW, Zhang YW, Liu ZR. Reciprocal regulation of protein kinase and pyruvate kinase activities of pyruvate kinase M2 by growth signals. J Biol Chem 2013; 288: 15971-15979.
[15] Li Y, Tang Y, Ye L, Liu B, Liu K, Chen J, Xue Q. Establishment of a hepatocellular carcinoma cell line with unique metastatic characteristics through in vivo selection and screening for metastasis-related genes through cDNA microarray. J Cancer Res Clin Oncol 2003; 129: 43-51.
[16] Yang W, Zheng Y, Xia Y, Ji H, Chen X, Guo F, Lyssiotis CA, Aldape K, Cantley LC, Liu ZM. ERK1/2-dependent phosphorylation and nuclear translocation of PKM2 promotes the Warburg effect. Nat Cell Biol 2012; 14: 1295-1304.
[17] Kitamura K, Hatano E, Higashi T, Narita M, Seo S, Nakamoto Y, Yanabaka K, Nagata H, Taura K,Yasuchika K, Nitta T, Uemoto S. Proliferative activity in hepatocellular carcinoma is closely correlated with glucose metabolism but not angiogenesis. J Hepatol 2011; 55: 846-857.
[18] Wiranowska M, Ladd S, Moscinski LC, Hill B, Haller E, Mikecz K, Plaas A. Modulation of hyaluronan production by CD44 positive glioma cells. Int J Cancer 2010; 127: 532-542.
[19] Kothapalli D, Flowers J, Xu T, Pure E, Assoian RK. Differential activation of ERK and Rac mediates the proliferative and anti-proliferative effects of hyaluronan and CD44. J Biol Chem 2008; 283: 31823-31829.
[20] Bourguignon LY, Wong G, Earle C, Krueger K, Spevak CC. Hyaluronan-CD44 interaction promotes c-Src-mediated twist signaling, microRNA-10b expression, and RhoA/RhoC up-regulation, leading to Rho-kinase-associated cytoskeleton activation and breast tumor cell invasion. J Biol Chem 2010; 285: 36721-36735.
[21] Kharaishvili G, Simkova D, Bouchalova K, Gachechiladze M, Narsia N, Bouchal J. The role of cancer-associated fibroblasts, solid stress and other microenvironmental factors in tumor progression and therapy resistance. Cancer Cell Int 2014; 14: 41.
[22] Feier D, Lupsor PM, Stefanescu H, Badea R. Transient elastography for the detection of hepatocellular carcinoma in viral C liver cirrhosis. Is there something else than increased liver stiffness? J Gastrointestin Liver Dis 2013; 22: 283-289.
[23] Chauhan VP, Boucher Y, Ferrone CR, Roberge S, Martin JD, Stylianopoulos T, Bardeesy N, DePinho RA, Padera TP, Munn LL, Jain RK. Compression of pancreatic tumor blood vessels by hyaluronan is caused by solid stress and not interstitial fluid pressure. Cancer Cell 2014; 26: 14-15.
[24] Provenzano PP, Cuevas C, Chang AE, Goel VK, Von Hoff DD, Hingorani SR. Enzymatic targeting of the stroma ablates physical barriers to treatment of pancreatic ductal adenocarcinoma. Cancer Cell 2012; 21: 418-429.
[25] Levine AJ, Puzio-Kuter AM. The control of the metabolic switch in cancers by oncogenes and tumor suppressor genes. Science 2010; 330: 1340-1344.
[26] Tamada M, Suematsu M, Saya H. Pyruvate kinase M2: multiple faces for conferring benefits on cancer cells. Clin Cancer Res 2012; 18: 5554-5561.
[27] Kaul R, Saha P, Saradhi M, Prasad RL, Chatterjee S, Ghosh I, Tyagi RK, Datta K. Overexpression of hyaluronan-binding protein 1 (HABP1/p32/gC1qR) in HepG2 cells leads to increased hyaluronan synthesis and cell proliferation by up-regulation of cyclin D1 in AKT-dependent pathway. J Biol Chem 2012; 287: 19750-19764.
[28] Ni J, Cozzi PJ, Hao JL, Beretov J, Chang L, Duan W, Shigdar s, Delprado WJ, Graham PH, Bucci J, Kearsley JH, Li Y. CD44 variant 6 is associated with prostate cancer metastasis and chemo-/radioresistance. Prostate 2014; 74: 602-617.
[29] Heise RL, Stober V, Cheluvaraju C, Hollingsworth JW, Garantziotis S. Mechanical stretch induces epithelial-mesenchymal transition in alveolar epithelia via hyaluronan activation of innate immunity. J Biol Chem 2011; 286: 17435-17444.
[30] Tamura R, Yokoyama Y, Yoshida H, Imaizumi T, Mizunuma H. 4-Methylumbelliferone inhibits ovarian cancer growth by suppressing thymidine phosphorylase expression. J Ovarian Res 2014; 7: 94.
[31] Bourguignon LY, Earle C, Wong G, Spevak CC, Krueger K. Stem cell marker (Nanog) and Stat-3 signaling promote MicroRNA-21 expression and chemoresistance in hyaluronan/CD44-activated head and neck squamous cell carcinoma cells. Oncogene 2012; 31: 149-160.
[32] Jacobetz MA, Chan DS, Neesse A, Bapiro TE, Cook N, Frese KK, Feig C, Nakagawa T, Caldwell ME, Zecchini HI, Lolkema MP, Ljiang P, Kultti A, Thompson CB, Maneval DC, Jodrell DI, Frost GI, Shepard HM, Skepper JN, Tuveson DA. Hyaluronan impairs vascular function and drug delivery in a mouse model of pancreatic cancer. Gut 2013; 62: 112-120.

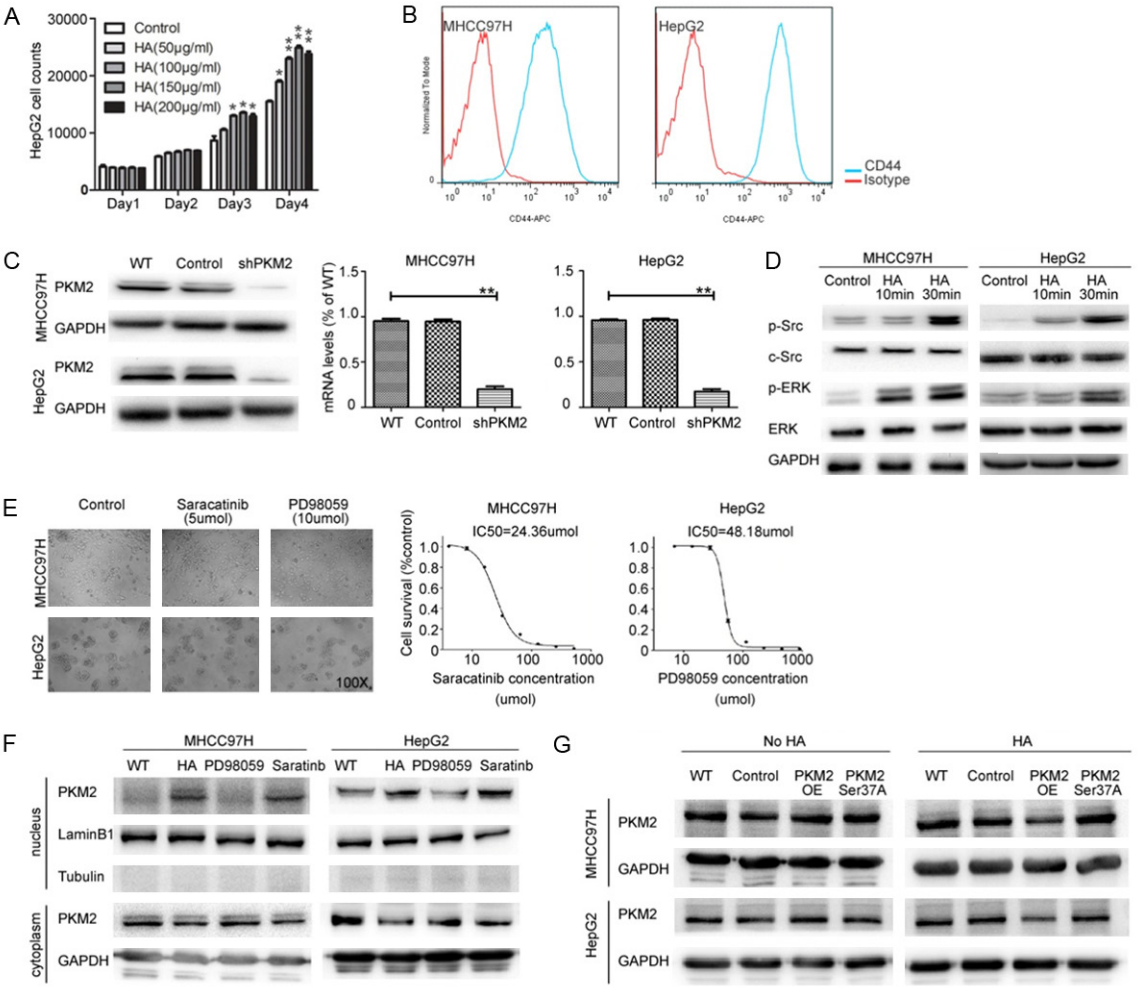


**Supplementary Figure 1.** A. Different concentrations of HA (50, 100, 150, 200 μg/ml) were included in the HepG2 cell proliferation assay. Compared with the control group, all four HA concentrations promoted the proliferation of HepG2 cells. B. A high percentage of cells were positive for CD44 in both MHCC97H and HepG2 cells. C. MHCC97H and HepG2 cells were transfected with lentivirus vectors, resulting in the stable knockdown of PKM2. D. c-Src and ERK were significantly activated at 30 minutes following HA stimulation. E. HCC cells were incubated for 6h with Saracatinib (4-500 μmol/ml) or PD98059 (7-900 μmol/ml) and the IC50 were calculated, which were much more than the kinase inhibiting concentration of those two drugs that had been reported previously. Treated HCC cells with Saracatinib or PD98059 at reported concentration did not affecting the morphology of the HCCs cells. F. Blocking ERK activation could inhibit HA-induced PKM2 nuclear translocation. G. Cytoplasm protein was extracted. PKM2 Ser37 mutation inhibited the nuclear translocation of PKM2.

## Supplementary materials and methods

*Lentivirus and tranfection*

Four lentiviruses were established by Hanyin Biotechnology, Shanghai, China: an empty vector control (Control), stable knockdown of PKM2 (shPKM2), overexpressed PKM2 (PKM2 OE), and a PKM2 Ser37A mutation (PKM2 Ser37A). All transfections were performed according to the manufacturer's protocols.

Stable knockdown of PKM2 (shPKM2) was accomplished using shRNA (5'-CATCTACCACTTGCAATTA-3') targeting the PKM2 exon 10 or a non-target shRNA control in pHY-LV-KD5.1 vector. Lentivirus targeting PKM2 was constructed with the full-length PKM2 cDNA cloned in pHY-LV-KD5.1 vector to overexpress PKM2 (PKM2 OE) or with an empty vector control.

PKM2 mutation (Ser37A) plasmid (vector pHY-LV-OE1.6) was amplified by over-lapping PCR products using the following primers: F: 5'-CCGGAATTCGCCACCATGGACTACAAGGACGATGACGACAAGTCGAAGCCCCATAGTGAAG-3'; R: 5'-CGGGATCCTCACGGCACAGGAACAACAC-3'; Mutant F: TGCCGCCTGGACATTGATGCACCACCCATCACAGCCC-3'; Mutant R: 5'-GGGCTGTGATGGGTGGTGCATCAATGTCCAGGCGGCAGGGCTGTGATGGGTGGTG-3'. Primers F/mutant R and mutant F/R were used for the first round of PCR independently, then the primer F/R with first round products as template were used for a second round of PCR to generate a full length mutation sequence [1].

*Preparation of whole cell lysates, subcellular fractionation and Western blot analysis*

The protocol was described in detail in previously by our lab [2]. Briefly, the whole-cell lysates were extracted using RIPA lysis buffer (Beyotime, China) containing PMSF and phosphatase inhibitor (Roche) at 4°C; The cytosol and nuclear extracts were prepared using NE-PER Nuclear and Cytoplasmic Extraction Reagents (Pierce Biotechnology). Protein samples were separated by 10% SDS-PAGE gel and transferred onto polyvinylidene difluoride membranes (Millipore). The membranes were blocked with 5% bovine serum albumin (BSA, Beyotime, China) for 2 hours, washed, and then incubated with primary antibodies overnight at 4°C at concentrations, which the manufacturer's protocol recommended. After washing, the membrane was incubated with appropriate HRP-conjugated secondary antibodies (Santa Cruz Biotechnology) and detected using enhanced chemiluminescence method (Pierce, IL). The amounts of proteins were quantified by densitometry with ImageJ software (National Institutes of Health, Bethesda, MD, USA) and normalized to relative internal standards. All of the experiments were performed in triplicate.

*Quantitative real-time PCR*

Total RNA was extracted using Trizol reagent. cDNA was synthesized from 500 ng RNA with PrimeScript RT Master Mix (Takara, Japan). Quantitative real-time PCR was performed using 2 × SYBR Green PCR Master Mix under the following conditions. 95°C for 30 seconds, followed by 40 cycles at 95°C for 5 seconds, 64°C for 34 seconds, and a melt cure step using a Step One Plus Real-Time PCR System (Applied Biosystems). The target gene expression levels for each experiment were normalized to GAPDH. The relative gene expression levels were detected and calculated by the Ct comparative method.

The RT-PCR primers used were as following. PKM2, 5'-GCTGCCATCTACCACTTGC-3' (forward) and 5'-CCAGACTTGGTGAGGACGATT-3' (reverse); GAPDH, 5'-GCACCGTCAAGGCTGAGAAC-3' (forward) and 5'-TGGTGAAGAACGCCAGTGGA-3'.

*Immunofluorescence*

PKM2 expression in HCC cell lines was detected using an immunofluorescence assay. Cells were treated with 4% formaldehyde and then permeabilized with 0.5% Triton X-100. Non-specific block binding was carried out with 5% BSA before incubation with the primary antibody (Anti-PKM2, ab137791 at 1:500 dilutions, Abcam, UK) overnight at 4°C. Secondary antibody (Alexa Fluor 594, Invitrogen, CA) was incubated at 37°C for 30 minutes. Nuclei were stained with DAPI (Roche) at 37°C for 5 minutes. Mouse

IgG was used as a negative control. Fluorescence microscopy (Leica Microsystems Imaging Solutions, UK) was used to observe the results.

*Cell proliferation and colony formation*

Cell proliferation was done as described [2]. In brief, 97H cells and G2 cells (4000 cells/well) were seeded into a 96-well plate. At the indicated time points, 100 μl Cell Kit-8 (Dojindo) was added to the cells for 2 hours, and then the plate was read using an enzyme-linked immunosorbent assay plate reader at 450 nm.

Cells were plated in 6-well plates at a density of 1000 cells/well and incubated for 14 days. The cells were fixed with 2% formalin for 10 minutes and stained with 0.5% crystal violet for 5 minutes prior to be photographed. Cell colonies with a diameter larger than 50 μm were counted using ImageJ software (National Institutes of Health, Bethesda, MD, USA).

*Cell migration and invasion*

Cell migration was evaluated using the scratch wound assay. Cells were cultured for 2 days to form a tight cell monolayer, which was then wounded with a 200 μl plastic pipette tip. Cultured by serum-free culture medium for 48 hours, migration cells at the wound front were photographed. Cell migration was calculated as percentages of cell coverage to the initial cell-free zone using ImageJ software. The values are the means of three independent experiments.

Transwell Permeable Supports (Corning, Lowell, MA, USA) with an 8-μm polycarbonate filter membrane was used, with 150 μg Matrigel (BD Biosciences, San Diego, CA, USA) coated on the top surface of the filter. Cells ($2 \times 10^4$ cells/well) with 150 μl serum-free medium were seeded into upper chamber of each well of a 24-well plate. And lower reservoir was filled medium containing 10% serum. After incubating 24 hours in normal conditions, the cells on the top surface were cleared physically, while the cells translocated the filter were stained and quantitated by visual inspection of the filter membranes.

*Measurements of aerobic glycolysis and pyruvate kinase activity*

Cells ($2 \times 10^5$) were seeded in 24-well plates, and the medium was changed after 6 h with serum free DMEM. Then, cells were incubated with the serum free DMEM with or without IM7 (20 μg/ml) or IgG (20 μg/ml) at 4°C for 30 minutes. Next, the medium was changed to 1 ml normal-serum DMEM with or without HA (100 μg/ml, Ultra Low Mw, GLR003, R&D systems) for 12 h, and then the medium was collected for measurement of glucose and lactate concentrations. A lucose assay kit and Lactate assay kit (MAK013 and MAK064, Sigma-Aldrich, USA) were used to determine the levels of glucose and lactate respectively. Glucose consumption was the difference in glucose concentration when compared with DMEM. The activity of PK was measured with a Pyruvate kinase assay (MAK072, Sigma-Aldrich, USA) according to the manufacturer's instruction.

*Evaluation of tumor growth in vivo*

The animal experiments were carried out in accordance with the guideline of the Shanghai Medical Experimental Animal Care Commission and all animals received human care. Male BALB/c nude mice (5 weeks old, Shanghai Institute of Materia Medica, Chinese Academy of Science) were housed under specific pathogen-free conditions. Twenty-four mice were randomized into four groups and cells ($5 \times 10^6$ per 200 μl Matrigel (1:8 diluted, 354263, BD Biosciences, CA) with 100 μg/ml HA (GLR003, R&D systems)) were subcutaneously injected. The tumor volumes were measured by vernier caliper every week, and the mice were euthanized after 4 weeks. The tumor volume was calculated by (large diameter) × (small diameter)$^2$/2.

*Flow cytometry*

Cells ($2 \times 10^5$) were stained with directly labeled mouse monoclonal antibodies directed against CD44 (APC-conjugated) in 0.1 ml PBS containing 0.1% bovine serum albumin for 30 minutes at 4°C. Non-

specific IgG was used as a negative control. FACScaliber Flow cytometer (BD Biosciences) and FlowJo software (Tree Star Inc, Ashland, Ore) were used to analyze the stained cells.

*Tissue microarray construction*

Tissue microarrays (TMAs) were generated in our previous reports [3]. Briefly, representative areas of tumor and adjacent normal tissue were circled away from the necrotic, hemorrhagic and major fibrotic areas. Triplicates of 1-mm diameter cylinders were cored from the areas of interest in the donor blocks and inserted into a recipient paraffin block in a grid pattern using a tissue arrayer (Beecher Instruments, Silver Spring, MD, USA). Sections (4 μm) were then cut from each recipient paraffin block.

## References

[1] Yang W, Zheng Y, Xia Y, Ji H, Chen X, Guo F, Lyssiotis CA, Aldape K, Cantley LC, Lu Z. ERK1/2-dependent phosphorylation and nuclear translocation of PKM2 promotes the Warburg effect. Nat Cell Biol 2012; 14: 1295-1304.

[2] Li JC, Yang XR, Sun HX, Xu Y, Zhou J, Qiu SJ, Ke AW, Cui YH, Wang ZJ, Wang WM, Liu KD, Fan J. Up-regulation of Kruppel-like factor 8 promotes tumor invasion and indicates poor prognosis for hepatocellular carcinoma. Gastroenterology 2010; 139: 2146-2157.

[3] Shi JY, Yang LX, Wang ZC, Wang LY, Zhou J, Wang XY, Shi GM, Ding ZB, Ke AW, Dai Z, Qiu SJ, Tang QQ, Gao Q, Fan J. CC Chemokine Receptor like 1 Functions as a Tumor Suppressor by Impairing CCR7-related Chemotaxis in Hepatocellular Carcinoma. J Pathol 2015; 235: 546-58.